Biosensors and Bioelectronics 240 (2023) 115664

Contents lists available at ScienceDirect

Biosensors and Bioelectronics

journal homepage: www.elsevier.com/locate/bios

Direct real-time measurements of superoxide release from skeletal muscles in rat limbs and human blood platelets using an implantable Cytochrome C microbiosensor

Aaditya S. Deshpande [a], Wayne Muraoka [b], James Wait [c], Arzu Çolak [c], Silvana Andreescu [a,*]

[a] Department of Chemistry and Biomolecular Science, Clarkson University, 8 Clarkson Avenue, Potsdam, NY, 13699-5810, USA
[b] U.S. Army Institute of Surgical Research, Blood and Shock Resuscitation, Fort Sam Houston, TX, 78234, USA
[c] Department of Physics, Clarkson University, 8 Clarkson Avenue, Potsdam, NY, 13699, USA

ARTICLE INFO

Keywords:
Superoxide
Cytochrome *c* biosensor
Ischemia-reperfusion
Human blood platelets
Conductive AFM

ABSTRACT

Oxidative stress and excessive accumulation of the superoxide ($O_2^{\cdot-}$) anion are at the genesis of many pathological conditions and the onset of several diseases. The real time monitoring of ($O_2^{\cdot-}$) release is important to assess the extent of oxidative stress in these conditions. Herein, we present the design, fabrication and characterization of a robust ($O_2^{\cdot-}$) biosensor using a simple and straightforward procedure involving deposition of a uniform layer of L-Cysteine on a gold wire electrode to which Cytochrome C (Cyt *c*) was conjugated. The immobilized layers, studied using conductive Atomic Force Microscopy (c-AFM) revealed a stable and uniformly distributed redox protein on the gold surface, visualized as conductivity and surface topographical plots. The biosensor enabled detection of ($O_2^{\cdot-}$) at an applied potential of 0.15 V with a sensitivity of 42.4 nA/μM and a detection limit of 2.4 nM. Utility of the biosensor was demonstrated in measurements of real time ($O_2^{\cdot-}$) release in activated human blood platelets and skeletal rat limb muscles following ischemia reperfusion injury (IRI), confirming the biosensor's stability and robustness for measurements in complex biological systems. The results demonstrate the ability of these biosensors to monitor real time release of ($O_2^{\cdot-}$) and estimate the extent of oxidative injury in models that could easily be translated to human pathologies.

1. Introduction

Oxidative stress and excessive reactive oxygen species (ROS) accumulation are at the genesis of many pathological conditions. Overproduction of ROS can induce oxidative damage to proteins, DNA, cells, and tissues, which has been associated with many pathologies, including cancer, neurodegeneration, cardiovascular and pulmonary diseases. The superoxide anion ($O_2^{\cdot-}$) generated due to cellular metabolism is one of the primary species in the broad ROS family. Studying of the role, amount, and dynamics of free radicals present and/or overexpressed in biological systems is of great interest in understanding their contribution on the onset and progression of these conditions. Because ROS production occurs very early in the progression of diseases, real-time detection and measurement of ROS can be used to evaluate oxidative stress conditions and therefore facilitate screening and treatment of those conditions. However, real time monitoring of ROS as an indicator of injury progression has been severely hampered by analytical difficulties. Due to their very short half-life (Murphy et al., 2022) and high reactivity, quantification of these reactive compounds in real time and following their progression in pathological conditions is very difficult. An even more challenging task is to perform such measurements directly in biological matrices, despite the increasing need to quantify oxidative status in many different conditions.

Conventional methods to detect reactive species include spectrophotometry (Ohyashiki et al., 1999), chemiluminescence (Ohara et al., 1993) and electron spin resonance (Mao and Poznansky, 1992). These methods involve indirect quantification, require long assay times, and provide only limited discrete endpoint information. Electrochemical detection using modified microelectrodes is one of the few available method that can directly quantify ROS *in situ*, due to its high sensitivity and temporal resolution. Unlike optical methods, electrochemical microsensors do not require addition of dyes or exogenous reagents for the detection of radicals, as the electron transfer is achieved by electrical means though immobilized redox reagents. Due to their small size,

* Corresponding author.
E-mail address: eandrees@clarkson.edu (S. Andreescu).

https://doi.org/10.1016/j.bios.2023.115664
Received 26 April 2023; Received in revised form 19 August 2023; Accepted 1 September 2023
Available online 2 September 2023

measurements with these sensors can be performed *in vivo* and adapted to a variety of environments (Henderson et al., 2009), but probes that could assess continuously the evolution of ROS species in complex biological environments, cells and tissues with high sensitivity are not readily available.

Previous works on electrochemical biosensors for ROS involved the use of redox proteins and microelectrodes functionalized with Cyt *c* or superoxide dismutase (SOD) as biological receptors (Calas-Blanchard and Noguer, 2014; Deshpande et al., 2021). A good example has been the use of Cyt *c*-based detection that utilizes the ability of ($O_2^{\cdot-}$) anion radicals to reduce Cyt *c* immobilized at electrode surfaces (Beissenhirtz et al., 2004). Most reported Cyt *c*-biosensors have been developed on macro-electrode platforms and their functionality has been established with standards and buffer solutions. Few reports demonstrate applicability for measurements of ($O_2^{\cdot-}$) *in vivo* at the production site, making these sensors of limited utility in relevant biological settings. We have previously reported a Cyt *c* microbiosensor for ($O_2^{\cdot-}$) measurements in mice brain tissues and bacterial cultures (Ganesana et al., 2012; Liu et al., 2016). A self-assembled monolayer (SAM) of mixed thiols was used to facilitate direct electron transfer and measurement of the reduced Cyt *c* upon interaction with ($O_2^{\cdot-}$) (Ge and Lisdat, 2002) (Ispas et al., 2008; Winterbourn, 2008). The use of thiols for immobilizing enzymes onto gold electrodes through the affinity of thiols for gold, forming SAM layers is well-documented (Ge and Lisdat, 2002; Manning et al., 1998; Tolias et al., 1999). These monolayers consisting of either one type or a mixture of thiols with different chain lengths are typically used to attach redox proteins to electrode surfaces (Yates et al., 2018). While the use of thiols for immobilizing Cyt *c* has been well-documented (Chen et al., 2008; Ge and Lisdat, 2002; Manning et al., 1998; Tolias et al., 1999), these procedures are lengthy and often lacks reproducibility.

In this study, we describe a new straightforward approach to fabricate a Cyt *c* biosensor on gold wire electrodes for determining the real-time release of ($O_2^{\cdot-}$) during oxidative injury. In this design, L-cysteine, a small amino acid with a thiol side chain was used as covalent linker to attach Cyt *c* to the surface of the AuME. The new method enabled rapid attachment of Cyt *c* with increased stability and a more efficient electron transfer as compared to the traditionally used mixed thiol layers (Chen et al., 2008). The general design is presented in Fig. 1. In addition to establishing biosensing performance, this work describes detailed investigation of the coverage of the gold surface upon Cyt *c* immobilization using c-AFM at bare and protein-coated substrates, which enabled us to estimate the monolayer thickness and evaluate changes in conductivity due to thiol binding across the surface.

To demonstrate the utility of the biosensor to measure ($O_2^{\cdot-}$) in relevant biological systems and track the evolution of these species during oxidative injury, we have selected two models: an IRI model in skeletal muscle in rat limb and human blood platelets activated by various platelets agonists. Because ROS production occurs very early in the progression of IRI, real-time detection of ROS can provide a direct continuous monitoring of the oxidative load, and ROS can be used as an indicator of injury progression. This proof-of-concept work demonstrates a practical application of this biosensing technology. For example, platelet activation is a critical step to initiate hemostasis in actively bleeding patients and biosensors can be used to rapidly evaluate platelet function. Therefore, the technology may benefit transfusion outcomes in actively bleeding patients. Thus, using these biosensors, it is possible to monitor real time release of ($O_2^{\cdot-}$) and estimate the extent of oxidative injury in models that could easily be translated to human pathologies.

2. Experimental section

2.1. Materials and reagents

Gold wires (0.5 mm diameter) were obtained from World Precision Instruments. Silver conductive epoxy was purchased from MG chemicals. L-Cysteine was purchased from Aldrich. 1-Ethyl-3-(3-dimethylaminopropyl) carbodiimide hydrochloric acid (EDC) was obtained from AK Scientific. N-Hydroxysuccinimide (NHS) was purchased from Fluka. Cyt *c* from equine heart, hypoxanthine, uric acid, SOD, potassium phosphate monobasic and xanthine oxidase (XOD) from bovine milk were purchased from Sigma Aldrich. Potassium hydroxide was purchased from Fischer Scientific. Sodium phosphate dibasic was purchased from Spectrum. Phosphate buffer (PBS) [0.1M] solutions at different pH values were prepared from sodium phosphate dibasic and potassium phosphate monobasic. All solutions were prepared with purified water (18 MΩ, Millipore, Direct-Q System).

2.2. Instrumentation

Electrochemical measurements were performed with a CH1030A electrochemical analyzer (CH Instruments Inc.) using a three-electrode electrochemical cell equipped with an Ag/AgCl/1M KCl reference electrode (CH111, CH Instruments Inc.) and a platinum wire counter electrode. The working electrode was a custom-made modified gold wire electrode having 0.5 mm diameter with a tip of 1 cm length exposed while the rest of the wire was insulated using Liquid Tape purchased from Goodfellows Inc. To fabricate the biosensor, the gold wires were incubated for all steps at 30 °C in an incubator from Boekel Instruments.

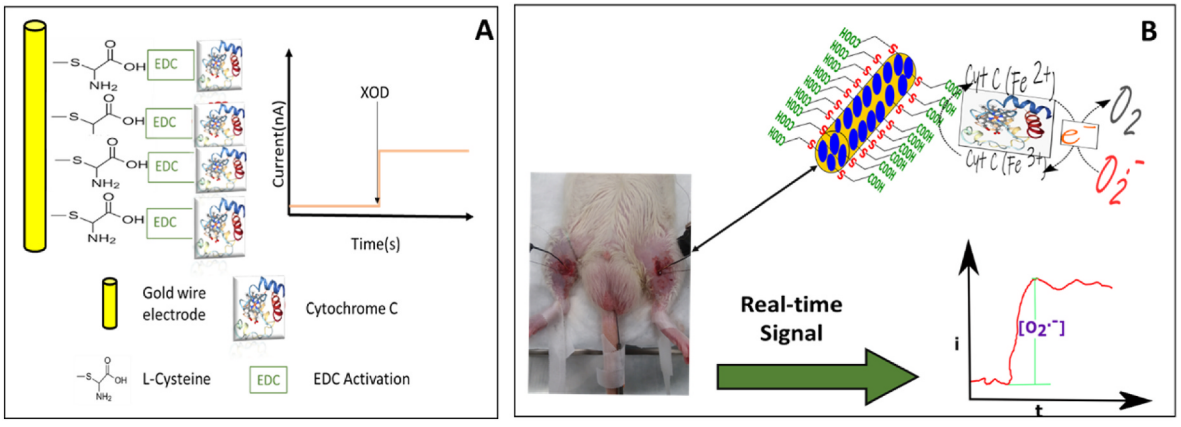

Fig. 1. Schematic showing the immobilization of Cyt *c* onto a gold wire electrode using L-Cysteine (A) and location of the biosensor implantation and measurements of the ($O_2^{\cdot-}$) release in rat limbs (B).

2.3. Biosensor fabrication

Gold wire electrodes (0.5 mm diameter) were chemically cleaned in piranha solution for ~15 min to remove the excess organics and then boiled in 2.5 M aq. KOH solution for ~30 min (Ge and Lisdat, 2002) after which the wire was electrochemically cleaned for 10 cycles at 100 mV/s from 0 V to 1.5V in 0.1M aq. H_2SO_4. Each electrode was verified to ensure that the last cycle gave the characteristic peaks expected for a clean gold electrode (Fig. S1). In case of unexpected peaks, the electrode was boiled again in KOH solution, electrochemically cleaned, and tested. The electrodes were carefully rinsed with DI water before further modification. Freshly cleaned electrodes were incubated in 100 mM L-cysteine for an hour to form a uniform L-cysteine monolayer on the surface. The next step was to activate the carboxylic acid terminal end of the L-cysteine by incubating the electrode for 1 h in a 100 mM EDC solution in 0.1M PBS (pH 6.5). The final immobilizing step was performed by incubating the electrodes in a 5 μM Cyt *c* solution prepared in 0.1M PBS (pH 6.5) for 2 h. The biosensors were rinsed with PBS and stored in 0.1 M PBS (pH 6.5) solution when not in use. To confirm modifications in the electrode surface and immobilization of the Cyt *c*, cyclic voltammograms (CV) were recorded in PBS after each step. For comparison, an alternative procedure in which the Cyt *c* was electrostatically immobilized is described in the supplementary information section (SI, S4). Surface coverage (Γ) of the electrode with redox-active Cyt *c* was calculated using the Laviron equation (Laviron, 1974, 1979) by integrating the reduction peak.

2.4. Superoxide measurements and biosensor calibration

Characterization of biosensor response was performed by single potential amperometry using enzymatically generated ($O_2^{\cdot-}$) $O_2^{\cdot-}$ in PBS (pH 6.5) at +0.15 V. The ($O_2^{\cdot-}$) radicals were generated *in situ* using XOD and its substrate hypoxanthine (HX) and biosensor calibration was obtained by measuring the response to XOD in the range 2.5–50 mU/mL in the presence of 100 μM HX. The current-time responses for increasing XOD concentrations were used to calibrate the biosensor and calculate the corresponding ($O_2^{\cdot-}$) concentrations, as described in SI, S2. The calibration obtained with the HX/XOD generated $O_2^{\cdot-}$ was used to estimate the ($O_2^{\cdot-}$) release.

2.5. AFM measurements

Before AFM measurements on the bare gold substrates with and without the Cyt *c*, the substrates were taken to a Nano indenter (TI950 Triboindenter, Hysitron Inc.). An L-shaped indentation was made on the surface of the bare gold substrate to scan the same area on the gold substrate before and after the redox Cyt *c* was deposited on the surface. The indentations were made 10 μm apart using a load of 5000 μN. This high load is indented deeply into the surface of the gold substrate, creating 600 nm indentations easily visible with the AFM microscope. The substrate was made electrically conductive by application of silver epoxy on the edge connecting the Au film side with the Si base side.

2.6. Biological experiments and biosensor implantation procedures

2.6.1. Hind-limb ischemia-reperfusion

This procedure was performed at the Army Medical Research Institute, Texas under IACUC protocol #A-20-028, ACURO # DM190422. e001. Rats were anesthetized with 2% isoflurane in an induction chamber and then maintained with 1.5–2.0% isoflurane with a nose cone during all procedures. The inguinal area was shaved and scrubbed with Betadine followed by ethanol. The rat was placed on a heated pad and body temperature was monitored with a rectal temperature probe (Harvard Apparatus, Holliston MA). A monofilament line, which served as a tourniquet, was wrapped around the right hind limb. The opposite end of the monofilament line was attached to a wire hook. A 3–5 mm incision was made in the skin over the gracilis muscle with fine iris scissors. The underlying muscle was exposed and an 18-gauge needle was used to pierce the muscle to a depth of 2 mm. The working, counter, and quasi reference electrodes were inserted into the muscle at a depth of 2 mm using a micromanipulator (World Precision Instruments, Sarasota FL). The left hind limb served as a control, which was instrumented but did not receive ischemia-reperfusion. Once instrumented, the rat was allowed to stabilize for 10 min. After stabilization, ischemia was established by adding an 89 g weight to the hook which applied tension to the monofilament line. Five minutes after adding the initial weight, an additional 30 g of mass was added to the hook and ischemia was maintained for 2 h. After the ischemic period, the weights were gradually removed from the hook over a period of 5 min, and the monofilament line was maintained in a relaxed state around the hind limb. Rats were maintained for an additional 4 h, then euthanized with Fatal Plus. Sham animals were instrumented, but no tension was applied to the monofilament line. Muscle tissue was collected in liquid nitrogen and stored at −80 °C until processing.

3. Results and discussions

3.1. Cyt c immobilization and bioelectrode characterization

The electrochemical detection of the ($O_2^{\cdot-}$) anion radical is based on the reaction between the Cyt *c* immobilized onto the gold wire electrode and the released ($O_2^{\cdot-}$) anions. Characterization of the Cyt *c* immobilization and biosensor performance was performed *in vitro* with enzymatically generated ($O_2^{\cdot-}$) (Arnold et al., 1997; Sato and Mizutani, 1997). A new immobilization chemistry using L-cysteine, a thiol amino acid, was employed in this work to covalently attach Cyt *c* onto the gold wire through the strong Au–S binding of cysteine to gold (Liu et al., 2007). Cysteine is a small molecule with three functional groups, –COOH, - NH_2 and –SH that facilitate interactions with metal surfaces though the –SH group (Li et al., 2006), as well as intramolecular hydrogen binding and covalent interactions suitable for protein attachment. Therefore, L-cysteine is an excellent bi-functional linker for protein immobilization and a promoter for fast electron transfer between the immobilized Cyt *c* and the gold surfaces (Liu et al., 2007). After L-cysteine immobilization, the carboxylic groups of L-cysteine were activated by incubation in a solution of EDC (0.1M PBS, 6.5 pH), which promotes covalent binding of Cyt *c*. Because of its low size, the use of L-cysteine provides a more homogenous monolayer-type structure, characterized in the next section by conductive AFM, as well as a rapid electron transfer between the redox protein and the gold surfaces as compared to the more conventionally used mixed thiols (Ganesana et al., 2012; Ge and Lisdat, 2002). Once immobilized, the covalently fixed Cyt *c* is reduced by the ($O_2^{\cdot-}$) and further re-oxidized at the electrode surface, generating an anodic current proportional to the ($O_2^{\cdot-}$) concentration.

To characterize the biosensor, the modification of the gold electrode at each step was confirmed by CV, as shown in Fig. 2. The CV of the cleaned bare Au shows characteristics peaks (Fig. S1), corresponding to the electrochemical processes of a typical gold electrode. No redox peaks were observed when the electrode was coated with L-cysteine and further with EDC. After Cyt *c* binding, a reversible redox couple corresponding to the oxidation and reduction of Cyt *c* is present at 0.15/-0.15 V, indicating direct redox behavior of Cyt *c* at the l-cysteine electrode. This peak remains stable even after multiple cycling and washing with PBS, confirming the presence and stability of the Cyt *c* on the gold electrode. To evaluate the nature of the electrode process, CVs of the Cyt *c* functionalized electrode were further recorded at various scan rates to determine the electron transfer kinetics. These measurements were carried out in 0.1 M PBS at pH 7.5 and scan rates of 10, 20, 50, 100, 150 and 200 mV/s. The oxidation and reduction peak currents for both the cathodic and anodic current recorded at +0.1 V and −0.1 V were

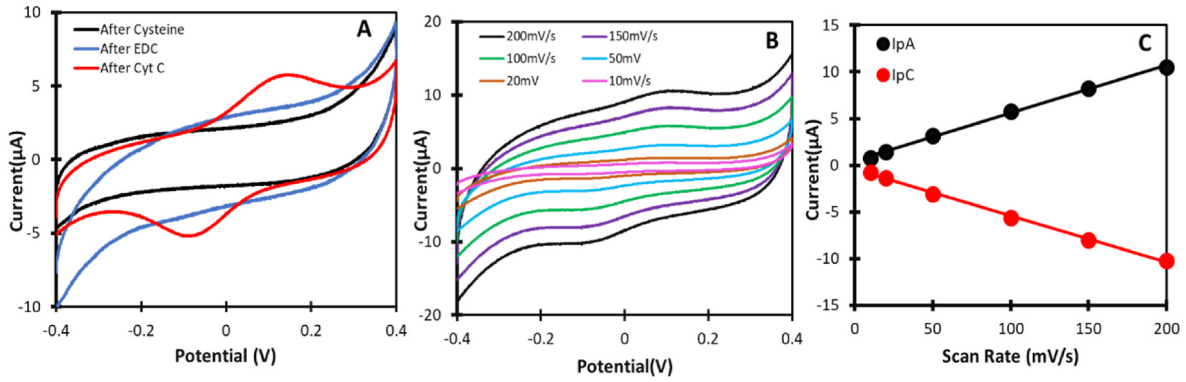

Fig. 2. (A) CVs of the gold wire electrode in 0.1 M PBS, pH 7.5 at 100 mV/s after each modification step, before and after functionalization with L-cysteine, EDC, and Cyt *c*.(B) CVs recorded in 0.1M PBS buffer at different scan rates of 10, 20, 50, 100, 150, 200 mV/s. (C) The effect of peak current with increasing scan rate giving a linear relationship with a R^2 of 0.9913.

linearly proportional with the scan rate, demonstrating a surface confined single electron redox process of the Cyt *c* and confirming the stability of the L-cysteine-supported Cyt *c* immobilization (Eckermann et al., 2010; Tian et al., 2002). By comparison, simple electrostatic adsorption of Cyt C onto the L-cysteine displayed a non-linear increase of the peak current as a function of scan rate.

The effect of different pH values (7.5, 6.5 and 5.5) on the effectiveness of the immobilization was further studied. It was observed that the use of a pH of 7.5 in the incubation solution was not favorable to Cyt *c* immobilization as no peaks were recorded. By comparison, physical immobilization of the Cyt *c* (fabrication described in SI) provided low intensity of the Cyt *c* peaks and the response was not stable. No redox peaks were observed when the same functionalization procedure was conducted on bare gold, without L-cysteine. The most stable redox peaks and the highest current intensities were obtained by incubating the electrode in PBS at a pH of 6.5. Table S1 summarizes the electrochemical properties of covalently immobilized Cyt *c*, e.g., the formal potentials and surface coverage at different pH values, for the bare and modified electrodes. The amount of the Cyt *c* immobilized on the surface of electrode ($\Gamma^{o}_{Cyt\ C}$) was calculated by integrating the peak for the

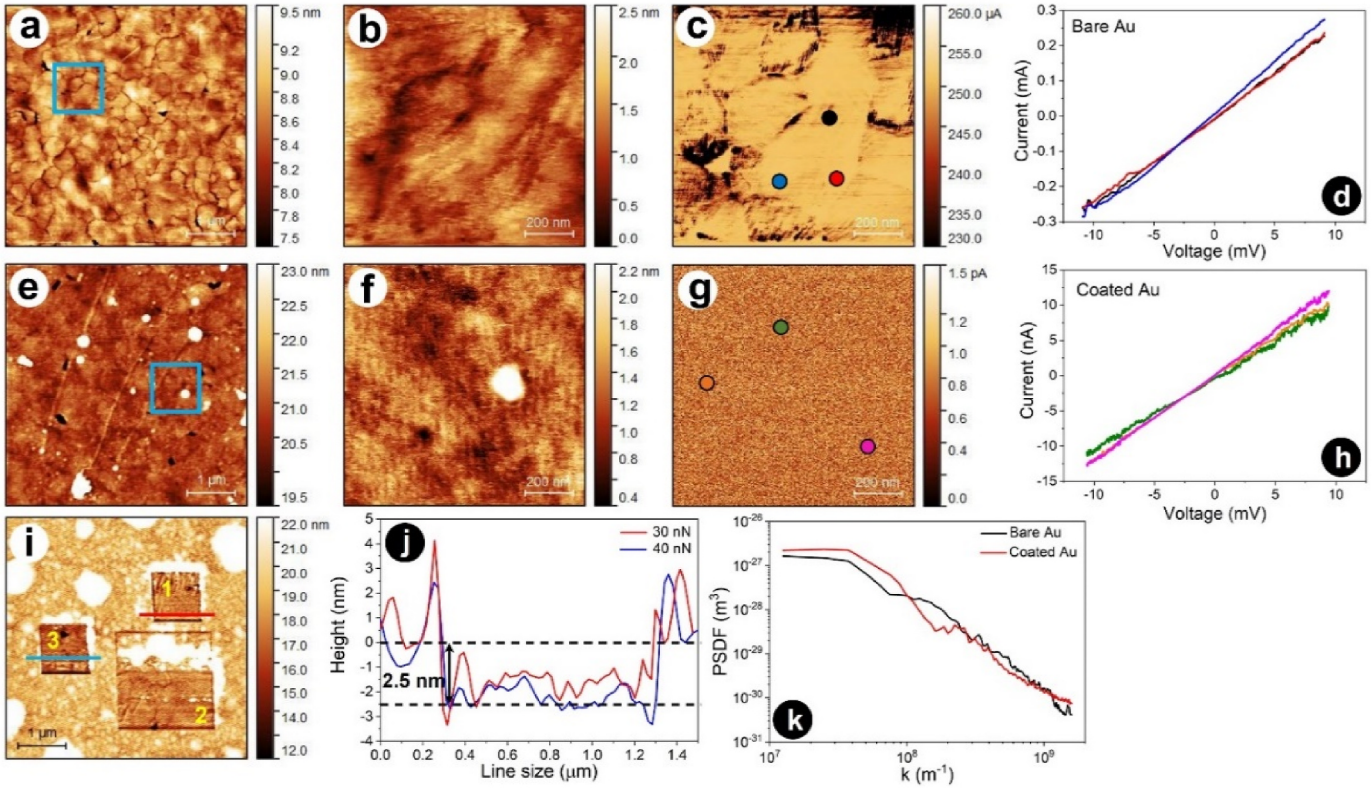

Fig. 3. c-AFM results for bare and coated gold (Au) substrates. For bare Au: (a–b) topography images, (c) corresponding local current map of area in (b) at an external bias of 25 mV, (d) local current-voltage graphs obtained at the three locations shown in (c). For coated Au: (e–f) topography images, (g) corresponding local current map of area in (f) at an external bias of 25 mV, (h) local current-voltage graphs obtained at the three locations shown in (g). (i) Topography of coated Au sample after scratched with an AFM tip at three different locations with 30 nN, 35 nN, and 40 nN loads, labeled as 1, 2, and 3, respectively, (j) line profiles of the scratches in (i) for 30 nN loads (red) and 40 nN loads (blue) showing a depth of 2.5 nm (k) the logarithm of the power spectral density (PSD) function of the surface roughness of bare Au (black) and coated Au (red) plotted as a function of the logarith of the inverse length scale. The blue squares in (a, e) highlight subsequent AFM scans' location in (b, f).

reduction cycle at 100 mV/s scan rate (Eckermann et al., 2010). For comparison, the redox parameters of the physically adsorbed Cyt *c* are also provided (Fig. S2). It was estimated that the coverage of the L-cysteine-modified Cyt *c* electrode was (1.93×10^{-10} mol cm^{-2}) indicating a monolayer structure with higher coverage than those reported for Cyc *c* immobilized using mixed SAM thiols, or (3.17×10^{-11}) and (9.2×10^{-12} pmol cm^{-2}) (Ge and Lisdat, 2002) respectively. The low ΔE_p values for all the three conditions did not match the theoretical value of 90.6, likely due to neighboring interactions amongst the immobilized Cyt C (Eckermann et al., 2010). Conductive AFM was further used to characterize the monolayer thickness and map the Cyt *c* distribution and coverage on the gold surface.

3.2. AFM characterization of the surface morphology of the gold substrate functionalized with Cyt c via L-cysteine

AFM measurements were conducted to study the surface topography and localization of the Cyt *c* on the gold substrate. Ultra-flat Au (111) surfaces were used for these tests. Prior scanning, the gold was thoroughly cleaned, and the surface was modified with Cyt *c* as described in the experimental section. In parallel with AFM measurements, the presence of Cyt *c* upon electrode modification was also confirmed by recording a CV of the Au substrate to verify the characteristic redox peaks of the Cyt *c*, as shown in Fig. 2. The surface topography and corresponding local current maps of the bare and Cyt *c* coated Au substrates characterized by AFM and the results are summarized in Fig. 3. Initially, 5 μm × 5 μm topography scans were recorded (Fig. 3 a, 2e) to understand the overall surface morphology of the bare and the coated Au substrates. With subsequent 1 μm × 1 μm topography scans (Fig 3.3b and 2f) the RMS (root mean square) roughness was determined as 0.30 nm and 0.36 nm for the bare and Cyt C coated Au substrates, respectively, which demonstrates that the Au surface morphology was unaltered after coating with the protein layer. To investigate the impact of Cyt C immobilization on the conductivity of Au, 1 μm × 1 μm current maps (Fig. 3c, 2g) as well as local current-voltage graphs (Fig 3.2d and 2h) of both bare and Cyt C coated Au surfaces were recorded. Comparing the current maps and local IV curves, it is concluded that the Cyt C immobilization decreases the conductivity of Au 10^5-fold. Such a dramatic decrease in conductivity raises a question regarding the thickness of the protein coating on Au surface, even though the surface morphology was unaltered after coating with the protein as the RMS roughness was the same.

To determine the thickness of Cyt *c* coating, the coated Au sample was scratched by scanning in the contact mode of AFM with applied loads of 30 nN, 35 nN, and 40 nN in the square shaped areas shown in Fig. S3, and labeled as 1, 2, and 3, respectively. In the scratched areas, the underlying bare gold grains became visible as the enzyme was removed, and a height difference was observed between the scratched areas and the surrounding areas coated with the enzyme. From the line profiles (red and blue lines in 2i), the step height was measured as 2.5 nm (2j, the height difference between black dashed lines), which gives the thickness of the immobilized enzyme coating. The Cyt *c* is a three-dimensional entity with a height of 2.5 nm (Beveridge and Graham, 1991), and it was attached to the bare Au surface with a monolayer of L-cysteine having length of ~6 Å (Heyrovska, 2011); therefore the expected thickness of a monolayer coating is about 3 nm. For this reason, it can be concluded that the measured step height of 2.5 nm with AFM reveals that the decrease in current is caused by a monolayer thick coating on Au surface. To explore the homogeneity of the monolayer coating on Au surface, the PSD of scanned images in (2b), and (2f) were compared as in (2k) in Fig. S3. The PSD describes the spatial distribution of surface roughness by showing which lateral frequencies contribute to the surface profile. The PSD spectrum of both bare and coated Au surface shows a very similar behavior especially at higher frequencies suggesting that the overall structure of both substrates is similar, hence the coating should be uniform on bare Au surface as it did not change the overall PSD. The uniformity of the coating suggests that Cyt *c* is uniformly deposited in a monolayer everywhere on the Au surface.

3.3. Biosensor calibration and characterization

3.3.1. Biosensor calibration and selectivity of measurements

Calibration of the Cyt *c* biosensor to quantitatively determine ($O_2^{\cdot-}$) was established by amperometry at a potential of 0.15 V vs. Ag/AgCl. Biosensor calibration was first obtained in buffer solutions with ($O_2^{\cdot-}$) radicals generated using XOD, a known oxidase enzyme catalyzing the HX oxidation in the presence of oxygen, generating ($O_2^{\cdot-}$) and uric acid, as shown in SI, Section S2. When ($O_2^{\cdot-}$) is generated, the Cyt *c* biosensor records a steady-state signal due to the steady formation of the ($O_2^{\cdot-}$), which is proportional to the square root of XOD (McCord and Fridovich, 1968), enabling calculation of the ($O_2^{\cdot-}$) concentration (S2, SI). Fig. 4 shows the amperometric responses generated upon additions of XOD to a cell containing 100 μM HX in PBS. With each XOD addition, the amperometric current increases and stabilizes within a few seconds. A sensitivity of 42.4 nA/μM or 1.3174×10^3 $a.m.^{-1}m^{-2}$ was calculated (n = 3), which is higher than that reported with Cyt C biosensors fabricated using mixed thiols (11.78 nA/μM) (Ganesana et al., 2012). The linear range of this biosensor covers the 0.2–0.8 μM concentration range and the limit of detection (LOD), calculated according to the 3σ/m criteria where m is the slope of the calibration curve and σ is the standard deviation of the blank, is 2.4 nM, lower than Cyt C biosensors based on mixed thiols (Deshpande et al., 2021; Ganesana et al., 2012).The limit of quantification (LOQ) is found to be 8.2 nM calculated using the 10 σ/m criteria where σ is the standard deviation and m is the slope of the calibration curve. The increased sensitivity of these L-cysteine biosensors versus those with mixed thiols can be attributed to the more uniform monolayer coverage and an enhanced electron transfer between the Cyt *c* and the gold electrode.

The biosensors were stable for up to five different measurements with no change in response when the same amount of ($O_2^{\cdot-}$) (0.33 μM) was generated in the cell (Fig. S4). The electrodes were stored in 0.1M PBS (7.5 pH) at 4 °C for up to seven days when not used. The selectivity of the biosensor was next studied first by addition of SOD, which is known to inactivate ($O_2^{\cdot-}$) by dismutation, thus inducing a decrease of the signal. When SOD was added to a solution containing ~0.15 μM theoretically calculated ($O_2^{\cdot-}$) at 37 °C, the response to ($O_2^{\cdot-}$) was rapidly suppressed and the signal decreased to a baseline level, indicating that the ($O_2^{\cdot-}$) radicals were completely inactivated by the added SOD (Fig. 4). Moreover, because uric acid (UA) is produced in the HX/XOD reaction that generate ($O_2^{\cdot-}$) as a side product, and UA is electrochemically active, the response to UA was also tested. When 50 μM UA was added to 100 μM HX, no signal was obtained. These results demonstrate the specificity of measurements for ($O_2^{\cdot-}$) and no interferences from the electroactive reaction by-product. The selectivity of the method is attributed to the low operating potential (−0.15 V vs Ag/AgCl), far from the typical oxidation potential of UA and HX (~0.46 V or higher, depending on the electrode (Patil et al., 2021)). This low operating potential also ensures selectivity against hydrogen peroxide. For comparison, experiments were also conducted with a Cyt *c* biosensor fabricated using mixed thiols as described previously, and the same trend was obtained, with the difference that the L-cysteine biosensor provided an enhanced signal to the same ($O_2^{\cdot-}$) concentration. It should also be noted that the time to fabricate the biosensors with L-cysteine is significantly reduced, as compared with the mixed thiols. Table S2 in SI provides a comparative summary of the performance of the biosensor described in this work and recently reported sensing design for ($O_2^{\cdot-}$) measurements in biological systems. We note that many of the previously reported sensors are developed on large electrodes such as glassy carbon that are not suitable for implantation, and most involve SOD-mimetic materials.

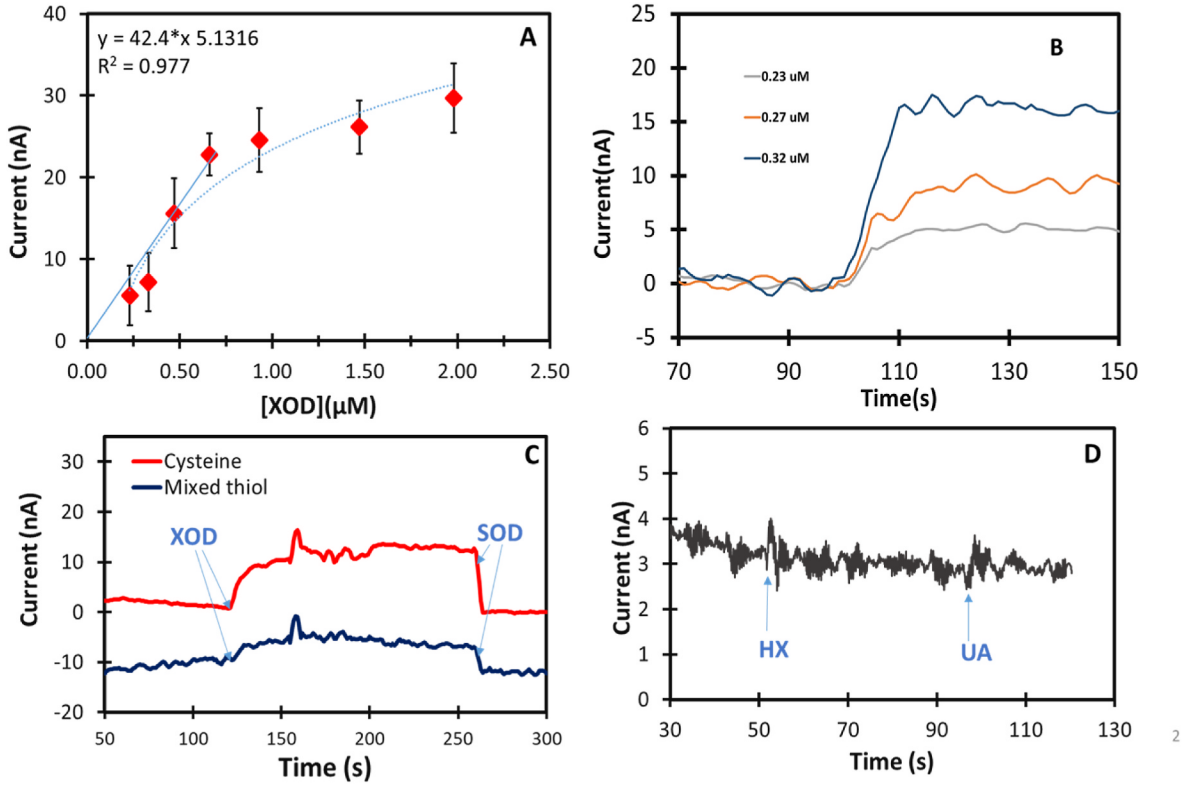

Fig. 4. (A) Calibration of the Cyt *c* biosensor in response to different ($O_2^{\cdot-}$) concentrations (calculated from the corresponding XOD) recorded in 0.1 M PBS at pH 7.5 (n = 3) at 0.15 V. (B) Amperometric responses to different concentrations of XOD in Tyrode's medium where 1, 3 and 5 correspond to 0.23, 0.27, 0.32 μM ($O_2^{\cdot-}$) respectively. (C) Effect of SOD addition on the signal. The decrease in signal clearly shows that the enzymatically generated ($O_2^{\cdot-}$) alone contributes to the generation of the signal. (D) Effect upon addition of HX (50 μM) and UA (100 μM) showing no interfering effects.

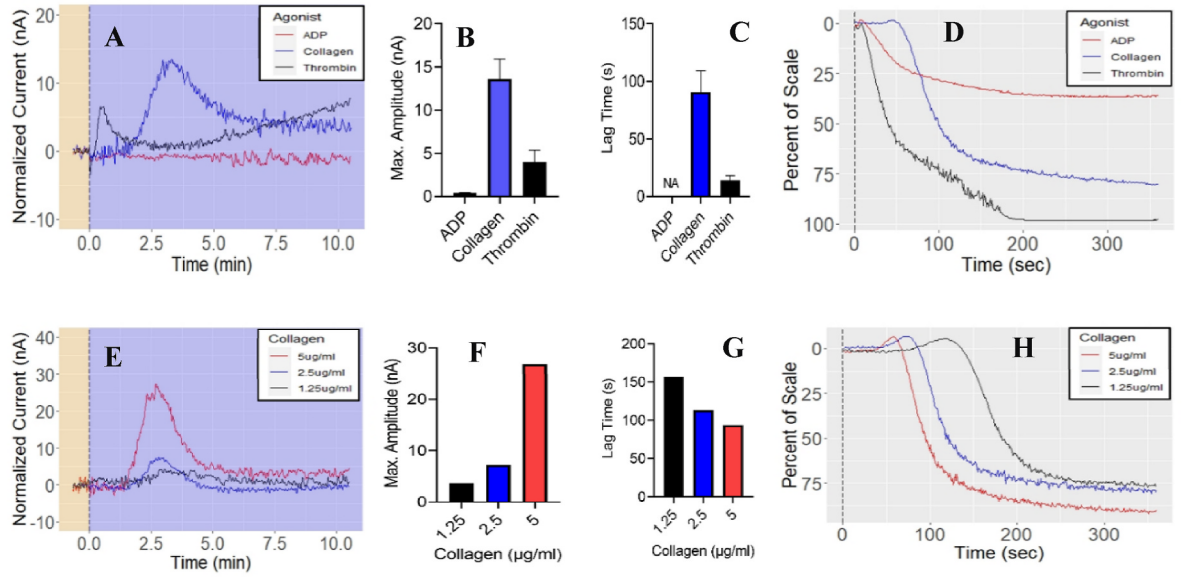

Fig. 5. Kinetics and magnitude of ROS evolution in activated human platelets. (A–D) Washed platelets were activated with either 10 μM ADP (black trace and bars), 5 μg/ml collagen (blue trace and bars), or 1 U/ml thrombin (black trace and bars). (A) Representative electrochemical detection of ROS when activated by various platelet agonists (t = 0 s). Current was normalized to the mean signal prior to activation and readings are shown after stabilization of the signal indicated by yellow bar. (B, C) Amplitude and lag time of ROS signal after activation with various agonists. (D) Light transmission aggregometry (LTA) of platelets from the same donor as A. (E–H) Washed platelets were activated with varying concentrations of collagen. (E) Representative electrochemical detection of ROS when activated by collagen (t = 0 s). Current was normalized to the mean signal prior to activation. (F, G) Amplitude and lag time of ROS signal after activation. (H) LTA of platelets from the same donor as E.

3.3.2. Measurements in human blood platelets

Human blood consists of anucleate blood platelets cells whose primary function comprise of hemostasis in addition to responses against inflammation, serving responses for innate immunity and maintenance of the blood vascular system (Gianazza et al., 2020; Kim et al., 2021). Due to their size and proximity to the walls of blood vessels they form a plug after following a series of changes as a response to the damage in blood vessels preventing/regulating blood loss upon injury (Harrison, 2005). ROS including $O_2^{\cdot-}$ are produced during platelet activation process due to different agonists including collagen, thrombin but not Adenosine Diphosphate (ADP) (Fig. 5 A, B) (Masselli et al., 2020; Wachowicz et al., 2002).

To measure the changes in platelet function, Light Transmission Aggregometry (LTA) has been used as the gold standard (Vinholt et al., 2017). This technique relies on the principle of increased in transmission of light upon aggregation of the platelets by an agonist (reversible for ADP) (Born, 1962). The results are obtained as a function of transmission/optical density against time. The limitations of this method as well as others traditionally used are well documented (Chan et al., 2018; Harrison, 2005; Mansouritorghabeh et al., 2020). When compared against collagen and thrombin, the ADP gives the least amount of signal for $(O_2^{\cdot-})$ while collagen gives the highest Fig. 5A, B. There is a significant lag time towards the production of $(O_2^{\cdot-})$ which can give some insights towards ROS generation from platelets upon interaction with an agonist. Surprisingly the lag time and the amount of $(O_2^{\cdot-})$ shows concentration dependency for collagen. The responses give the values of $(O_2^{\cdot-})$ to be 0.27, 0.38, and 0.50 μM for the 1.25, 2.5 and 5 μg/mL collagen concentrations used (Fig. 5F). LTA measurements were carried out to support the findings of the electrochemical measurements Fig. 5A, E. The signals correspond to an amount of 0.306 μM and 0.282 μM of $(O_2^{\cdot-})$ for collagen and thrombin respectively whilst the signal for ADP was low (1.5 nA = 0.2 μM) (Fig. 5B). It should be noted that the calibration curve used Tyrode's as the medium and had a sensitivity of 121.4 nA/μM (n = 3) for the measurements related to Fig. 5B and 66.5 nA/μM (n = 3) for measurements related to Fig. 5F which was higher than that of PBS and can be attributed to the bicarbonate and phosphate salts present in Tyrode's solution which might increase the overall conductivity.

3.3.3. In vivo superoxide measurements in rat limbs skeletal muscles

Ischemia in general, means a lack of blood due to constricted arterial blood flow (Kalogeris et al., 2012) with the restoration of blood flow denoted by the term reperfusion. The restoration of blood flow has been linked to the onset of several conditions (Eltzschig and Eckle, 2011) due to an increase in inflammatory response and is known as ischemia-reperfusion injury (IRI) (Kuroda et al., 2020). A lot of research has focused on vital organs *viz.* brain, heart, kidneys affected by IRI including skeletal muscles (Gillani et al., 2012; Kuroda et al., 2020; Soares et al., 2019).The presence of $O_2^{\cdot-}$ in skeletal muscles has been shown to increase other ROS species by reaction pathways (Zhou et al., 2018). Indeed, our results showcase the same trends of increased $(O_2^{\cdot-})$ during reperfusion (Fig. 6). As expected, the sham animals did not show much change for $(O_2^{\cdot-})$ levels. The increase in current levels (~15 nA) during reperfusion shows the presence of $(O_2^{\cdot-})$ levels demonstrating that higher ROS is present upon the resumption of the blood flow and agree with the literature that IRI leads to oxidative stress causing cell damage (Wu et al., 2018). This demonstration shows that real time $(O_2^{\cdot-})$ monitoring in skeletal muscle could be used instead of imaging modality (Kuroda et al., 2020).

4. Conclusions

This work introduced a simple and straightforward procedure to immobilize Cyt *c* using a small natural amino acid with a thiol side chain, L-cysteine, which provided increased sensitivity and a shorter and more robust fabrication protocol. The work also established a new method to quantify thickness and distribution of redox protein layers on gold electrode surfaces using conductive cAFM. The developed procedure can be easily adapted to the study of other redox protein layers. The biosensor enabled $O_2^{\cdot-}$ measurements in human blood platelets and rat limbs to quantify kinetics and magnitude of $O_2^{\cdot-}$ production during IRI injury, demonstrating applicability in real world environments. This work opens avenues for further implementation of electrochemical biosensors to monitor ROS and quantify oxidative injury in conditions such as for example for example, platelet activation to rapidly evaluate platelet function and transfusion outcomes in actively bleeding patients. These biosensors can be used to study fundamental mechanisms to understand ROS-mediated injury in pathophysiological conditions and quantify real-time changes of ROS in disease progression and assessment of therapeutic interventions.

Disclaimer

The *in vivo* work described in this chapter was done at the U.S. Army Institute of Surgical Research, Blood and Shock Resuscitation, Fort Sam Houston, TX 78234, in collaborative work with Dr. Wayne Muraoka. The work was funded by the U.S. Army Medical Department, Department of the Army, DoD, or the U.S. Government. This work was funded by the U. S. Army Medical Department, Department of the Army, DoD by a congressionally Directed Medical Research Program grant (W81XWH2020054). The views expressed in this work are those of the author(s) and do not reflect the official policy or position of the U.S. Army Medical Department, Department of the Army, DoD, or the U.S. Government.

CRediT authorship contribution statement

Aaditya S. Deshpande: Methodology, Formal analysis,

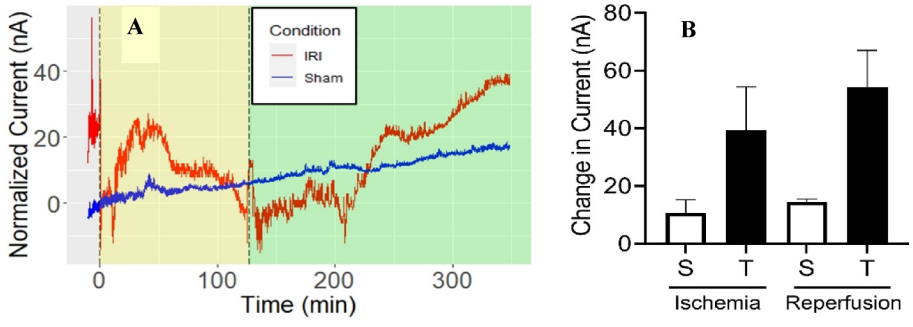

Fig. 6. Kinetics and magnitude of $(O_2^{\cdot-})$ evolution in a model of skeletal muscle ischemia and reperfusion. (A) Representative electrochemical detection of ROS when sensors were implanted into rat skeletal muscle subjected ischemia (yellow shaded area) and reperfusion (green shaded area) by tourniquet application (red trace, n = 2). Sham subjects (blue trace, n = 2) were instrumented with the sensor, but no tension was applied to the tourniquet. Shaded areas for the sham subject are for comparison purposes to the ischemic subject. Vertical dashed lines depict the application of tension to the tourniquet (t = 0) or release of tension from the tourniquet (t = 120). (B) S=Sham, T = Tourniquet. Amplitude of signal change during ischemia and reperfusion. Change in current was determined by subtracting the signal just after tourniquet application (t = 0) or tourniquet release (t = 120) from the maximum value during each respective phase.

Investigation, Writing – original draft, Visualization. **Wayne Muraoka:** Conceptualization, Methodology, Formal analysis, Investigation, Writing – original draft, Visualization, Project administration, Funding acquisition. **James Wait:** Methodology, Formal analysis, Methodology, Investigation, Writing – original draft. **Arzu Çolak:** Methodology, Formal analysis, Investigation, Supervision, Writing – original draft. **Silvana Andreescu:** Conceptualization, Supervision, Writing – review & editing, Project administration, Funding acquisition.

Declaration of competing interest

The authors declare that they have no known competing financial interests or personal relationships that could have appeared to influence the work reported in this paper.

Data availability

Data will be made available on request.

Acknowledgements

We acknowledge funding from the US -National Science Foundation grant (NSF 20425544) to SA. Any opinions, findings, and conclusions or recommendations expressed in this material are those of the author(s) and do not necessarily reflect the views of the National Science Foundation or the US Army.

Appendix A. Supplementary data

Supplementary data to this article can be found online at https://doi.org/10.1016/j.bios.2023.115664.

References

Arnold, S., Feng, Z.Q., Kakiuchi, T., Knoll, W., Niki, K., 1997. Investigation of the electrode reaction of cytochrome c through mixed self-assembled monolayers of alkanethiols on gold(111) surfaces. J. Electroanal. Chem. 438 (1–2), 91–97.
Beissenhirtz, M.K., Scheller, F.W., Lisdat, F., 2004. A superoxide sensor based on a multilayer cytochrome c electrode. Anal. Chem. 76 (16), 4665–4671.
Beveridge, T.J., Graham, L.L., 1991. Surface layers of bacteria. Microbiol. Rev. 55 (4), 684–705.
Born, G.V.R., 1962. Aggregation of blood platelets by adenosine diphosphate and its reversal. Nature 194 (4832), 927–929.
Calas-Blanchard, C.C., Noguer, G., 2014. Electrochemical sensor and biosensor strategies for ROS/RNS detection in biological systems. Electroanalysis 26 (6), 1277–1286.
Chan, M.V., Armstrong, P.C., Warner, T.D., 2018. 96-well plate-based aggregometry. Platelets 29 (7), 650–655.
Chen, X.J., West, A.C., Cropek, D.M., Banta, S., 2008. Detection of the superoxide radical anion using various alkanethiol monolayers and immobilized cytochrome c. Anal. Chem. 80 (24), 9622–9629.
Deshpande, A.S., Muraoka, W., Andreescu, S., 2021. Electrochemical sensors for oxidative stress monitoring. Curr. Opin. Electrochem. 29, 100809.
Eckermann, A.L., Feld, D.J., Shaw, J.A., Meade, T.J., 2010. Electrochemistry of redox-active self-assembled monolayers. Coord. Chem. Rev. 254 (15), 1769–1802.
Eltzschig, H.K., Eckle, T., 2011. Ischemia and reperfusion—from mechanism to translation. Nat. Med. 17 (11), 1391–1401.
Ganesana, M., Erlichman, J.S., Andreescu, S., 2012. Real-time monitoring of superoxide accumulation and antioxidant activity in a brain slice model using an electrochemical cytochrome c biosensor. Free Radic. Biol. Med. 53 (12), 2240–2249.
Ge, B., Lisdat, F., 2002. Superoxide sensor based on cytochrome c immobilized on mixed-thiol SAM with a new calibration method. Anal. Chim. Acta 454 (1), 53–64.
Gianazza, E., Brioschi, M., Baetta, R., Mallia, A., Banfi, C., Tremoli, E., 2020. Platelets in healthy and disease states: from biomarkers discovery to drug targets identification by proteomics. Int. J. Mol. Sci. 21 (12), 4541.
Gillani, S., Cao, J., Suzuki, T., Hak, D.J., 2012. The effect of ischemia reperfusion injury on skeletal muscle. Injury 43 (6), 670–675.
Harrison, P., 2005. Platelet function analysis. Blood Rev. 19 (2), 111–123.
Henderson, J.R., Swalwell, H., Boulton, S., Manning, P., McNeil, C.J., Birch-Machin, M. A., 2009. Direct, real-time monitoring of superoxide generation in isolated mitochondria. Free Radic. Res. 43 (9), 796–802.
Heyrovska, R., 2011. Precise molecular structures of cysteine, cystine, hydrogen-bonded dicysteine, cysteine dipeptide, glutathione and acetyl cysteine based on additivity of atomic radii. Nat. Prec.
Ispas, C., Njagi, J., Cates, M., Andreescu, S., 2008. Electrochemical studies of ceria as electrode material for sensing and biosensing applications. J. Electrochem. Soc. 155 (8), F169–F176.
Kalogeris, T., Baines, C.P., Krenz, M., Korthuis, R.J., 2012. Chapter six - cell biology of ischemia/reperfusion injury. In: Jeon, K.W. (Ed.), International Review of Cell and Molecular Biology. Academic Press, pp. 229–317.
Kim, C.-J., Kim, J., Sabaté del Río, J., Ki, D.Y., Kim, J., Cho, Y.-K., 2021. Fully automated light transmission aggregometry on a disc for platelet function tests. Lab Chip 21 (23), 4707–4715.
Kuroda, Y., Togashi, H., Uchida, T., Haga, K., Yamashita, A., Sadahiro, M., 2020. Oxidative stress evaluation of skeletal muscle in ischemia–reperfusion injury using enhanced magnetic resonance imaging. Sci. Rep. 10 (1), 10863.
Laviron, E., 1974. Adsorption, autoinhibition and autocatalysis in polarography and in linear potential sweep voltammetry. J. Electroanal. Chem. Interfacial Electrochem. 52 (3), 355–393.
Laviron, E., 1979. General expression of the linear potential sweep voltammogram in the case of diffusionless electrochemical systems. J. Electroanal. Chem. Interfacial Electrochem. 101 (1), 19–28.
Li, Z.P., Duan, X.R., Liu, C.H., Du, B.A., 2006. Selective determination of cysteine by resonance light scattering technique based on self-assembly of gold nanoparticles. Anal. Biochem. 351 (1), 18–25.
Liu, X., Marrakchi, M., Jahne, M., Rogers, S., Andreescu, S., 2016. Real-time investigation of antibiotics-induced oxidative stress and superoxide release in bacteria using an electrochemical biosensor. Free Radic. Biol. Med. 91, 25–33.
Liu, Y.C., Cui, S.Q., Zhao, J., Yang, Z.S., 2007. Direct electrochemistry behavior of cytochrome c/L-cysteine modified electrode and its electrocatalytic oxidation to nitric oxide. Bioelectrochemistry 70 (2), 416–420.
Manning, P., McNeil, C.J., Cooper, J.M., Hillhouse, E.W., 1998. Direct, real-time sensing of free radical production by activated human glioblastoma cells. Free Radic. Biol. Med. 24 (7), 1304–1309.
Mansouritorghabeh, H., de Laat, B., Roest, M., 2020. Current methods of measuring platelet activity: pros and cons. Blood Coagul. Fibrinolysis 31 (7), 426–433.
Mao, G.D., Poznansky, M.J., 1992. Electron spin resonance study on the permeability of superoxide radicals in lipid bilayers and biological membranes. FEBS Lett. 305 (3), 233–236.
Masselli, E., Pozzi, G., Vaccarezza, M., Mirandola, P., Galli, D., Vitale, M., Carubbi, C., Gobbi, G., 2020. ROS in platelet biology: functional aspects and methodological insights. Int. J. Mol. Sci.
McCord, J.M., Fridovich, I., 1968. The reduction of cytochrome c by milk xanthine oxidase. J. Biol. Chem. 243 (21), 5753–5760.
Murphy, M.P., Bayir, H., Belousov, V., Chang, C.J., Davies, K.J.A., Davies, M.J., Dick, T. P., Finkel, T., Forman, H.J., Janssen-Heininger, Y., Gems, D., Kagan, V.E., Kalyanaraman, B., Larsson, N.-G., Milne, G.L., Nyström, T., Poulsen, H.E., Radi, R., Van Remmen, H., Schumacker, P.T., Thornalley, P.J., Toyokuni, S., Winterbourn, C. C., Yin, H., Halliwell, B., 2022. Guidelines for measuring reactive oxygen species and oxidative damage in cells and in vivo. Nat. Metab. 4 (6), 651–662.
Ohara, Y., Peterson, T.E., Harrison, D.G., 1993. Hypercholesterolemia increases endothelial superoxide anion production. J. Clin. Investig. 91 (6), 2546–2551.
Ohyashiki, T., Nunomura, M., Katoh, T., 1999. Detection of superoxide anion radical in phospholipid liposomal membrane by fluorescence quenching method using 1,3-diphenylisobenzofuran. Biochim. Biophys. Acta Biomembr. 1421 (1), 131–139.
Patil, A.B., Zheng, C., Ma, L., Wu, R., Mengane, S.K., Zhang, Y., Liu, X., Meng, Z., Zhang, W., Xu, Z., Chen, C., Huang, J., Liu, X.Y., 2021. Flexible and disposable gold nanoparticles-N-doped carbon-modified electrochemical sensor for simultaneous detection of dopamine and uric acid. Nanotechnology 32 (6), 065502.
Sato, Y., Mizutani, F., 1997. Electrochemical responses of cytochrome c on a gold electrode modified with mixed monolayers of 3-mercaptopropionic acid and n-alkanethiol. J. Electroanal. Chem. 438 (1–2), 99–104.
Soares, R.O.S., Losada, D.M., Jordani, M.C., Évora, P., Castro-e-Silva, O., 2019. Ischemia/reperfusion injury revisited: an overview of the latest pharmacological strategies. Int. J. Mol. Sci.
Tian, Y., Mao, L., Okajima, T., Ohsaka, T., 2002. Superoxide dismutase-based third-generation biosensor for superoxide anion. Anal. Chem. 74 (10), 2428–2434.
Tolias, C.M., McNeil, C.J., Kazlauskaite, J., Hillhouse, E.W., 1999. Superoxide generation from constitutive nitric oxide synthase in astrocytes in vitro regulates extracellular nitric oxide availability. Free Radic. Biol. Med. 26 (1), 99–106.
Vinholt, P.J., Nybo, M., Nielsen, C.B., Hvas, A.-M., 2017. Light transmission aggregometry using pre-coated microtiter plates and a Victor X5 plate reader. PLoS One 12 (10), e0185675.
Wachowicz, B., Olas, B., Zbikowska, H.M., Buczyński, A., 2002. Generation of reactive oxygen species in blood platelets. Platelets 13 (3), 175–182.
Winterbourn, C.C., 2008. Reconciling the chemistry and biology of reactive oxygen species. Nat. Chem. Biol. 4 (5), 278–286.
Wu, M.Y., Yiang, G.T., Liao, W.T., Tsai, A.P.Y., Cheng, Y.L., Cheng, P.W., Li, C.Y., Li, C.J., 2018. Current mechanistic concepts in ischemia and reperfusion injury. Cell. Physiol. Biochem. 46 (4), 1650–1667.
Yates, N.D.J., Fascione, M.A., Parkin, A., 2018. Methodologies for "wiring" redox proteins/enzymes to electrode surfaces. Chem. Eur J. 24 (47), 12164–12182.
Zhou, T., Prather, E.R., Garrison, D.E., Zuo, L., 2018. Interplay between ROS and antioxidants during ischemia-reperfusion injuries in cardiac and skeletal muscle. Int. J. Mol. Sci.